Instability Mediated Self-Templating of Drop Crystals

Lingzhi Cai¹, Joel Marthelot^{1,2} and P.-T. Brun¹

¹Department of Chemical and Biological Engineering,
Princeton University, Princeton, New Jersey 08540, USA,

²Aix-Marseille University, CNRS, IUSTI, 13013, Marseille, France
(Dated: May 13, 2022)

The breakup of liquid threads into droplets is prevalent in engineering and natural settings. While drop formation in these systems has a long-standing history, existing studies typically consider axisymmetric systems. Conversely, the physics at play when multiple threads are involved and the interaction of a thread with a symmetry breaking boundary remain unexplored. Here we show that the breakup of closely spaced liquid threads sequentially printed in an immiscible bath locks into crystal like lattices of droplets. We rationalize the hydrodynamics at the origin of this previously unknown phenomenon. We leverage this knowledge to tune the lattice pattern via the control of injection flow rate and nozzle translation speed, thereby overcoming the limitations in structural versatility typically seen in existing fluid manipulations paradigms. We further demonstrate that these drop crystals have the ability to self-correct and propose a simple mechanism to describe the convergence towards a uniform pattern of drops.

Introduction

In the Rayleigh-Plateau instability of a flowing jet, interfacial perturbations can be modeled as exponential functions with complex frequencies and wavelengths whose superposition generates wave packets that travel both up and downstream until the thread breaks to generate drops [1-4]. Depending on the setting, these droplets are the vehicle for biological material, drugs, polymeric solutions or are destined to combustion, while their radius may range anywhere from a few millimeters to tenth of nanometers [5–10]. In addition to its applicability, the breakup of jets illustrates key phenomena in the physics of fluids, e.g. absolute/convective instabilities, singularities. As such, the Rayleigh-Plateau instability has been extensively studied, albeit primarily in the context of a single jet and assuming axisymetry [4]. Therefore, little is known on the collective stability of multiple threads [11–13]; in particular the case of the successive breakups of neighboring jets has never been reported. Here we show that viscous threads sequentially extruded into another immiscible viscous bath lead to the self-assembly of complex droplet lattices. This self-templating effect is underpinned by the noise amplifier nature of the instability that turns the infinitesimal perturbations of the interface of a thread into drops [14, 15]. Here, perturbations in a given thread are inherited from breakup events in previously extruded threads, thereby slowly building up memory in the system which eventually converges towards a crystalline structure. With our technique, the size of droplets and their arrangements are fully controlled by fluid dynamics. While packed hexagonal lattices are routinely used in top down fabrication methods [16–19], the flexibility of our approach allows for the assembly of previously impossible complex arrays, which can subsequently be polymerized as a route to design functional materials [20–24]. More generally, these droplet assemblies could find widespread application in many fields, including microbiology [25–27], tissue engineering [28], acoustics [29, 30],

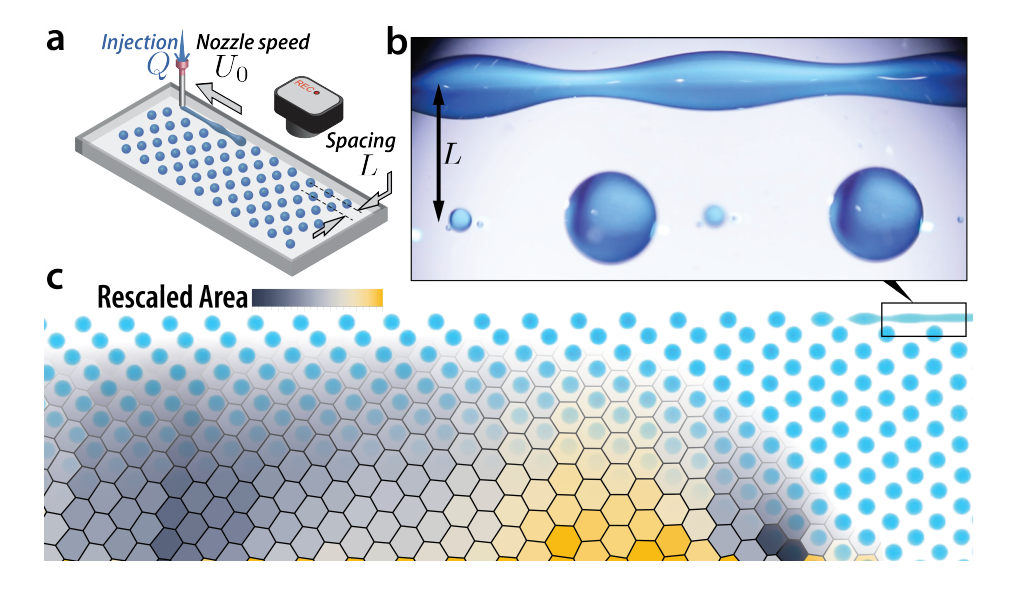


FIG. 1. Sequential breakup of viscous threads. (a) Schematic of the experimental setup: glycerol is injected from a nozzle into a reservoir of silicone oil. A jet develops at the nozzle outlet and breaks up into droplets due to the Rayleigh-Plateau instability. (b) Close-up photograph showing the developing troughs and peaks along the jet next to the adjacent droplets. (c) Snapshot of the printing experiment with nozzle speed $U_0 = 4.7 \text{ mm/s}$, flow rate Q = 0.21 mL/min and spacing L = 3.0 mm. The rows are printed in alternating directions and the drops progressively arrange into an ordered lattice. Overlaid is the Voronoi tessellation obtained from the drop centroids and color coded using the relative area of each cell.

optics [31, 32] and electrical components [33, 34].

Results

In Fig. 1a, we show our printing system where glycerol is injected through a moving nozzle into an immiscible silicone oil bath to form a liquid jet. The jet follows the trajectory of the nozzle before it breaks into droplets. In this article we show that the printing process builds on the hydrodynamical interaction of a thread with the surrounding environment (Fig. 1b). In particular, the sequential deposition and breakup process gives rise to a crystal-like lattice of droplets as evident in Fig. 1c (see Supplementary Video 1). As evident from the Voronoi diagram overlaid on the figure, the array gets more uniform as more rows are added and the defects present in the first lines are progressively smoothed out.

To elucidate the physics at play in our problem we develop model experiments involving solid templates designed to emulate the presence of nearby droplets. In Fig. 2a, we show a photograph of an experiment where a liquid jet is breaking up near a solid template with wavelength λ^* matching that of the Rayleigh-Plateau instability [35] (see Supplementary Video 2). The value of λ^* scales with the radius of the injected jet, h_0 , in turn determined by mass conservation, $h_0 = \sqrt{Q/(\pi U_0)}$, where Q is the injection flow rate and U_0 the speed of the nozzle [10]. Geometry is anticipated to matter here, i.e., the relative magnitude of the distance to template L and h_0 . In particular, in Fig. 2b we show that when L decreases, the standard deviation in the observed breakup wavelength λ decreases too, as indicated by the size of error bars. We also find that with $L/h_0 \leq 8$ the standard deviation in wavelength is

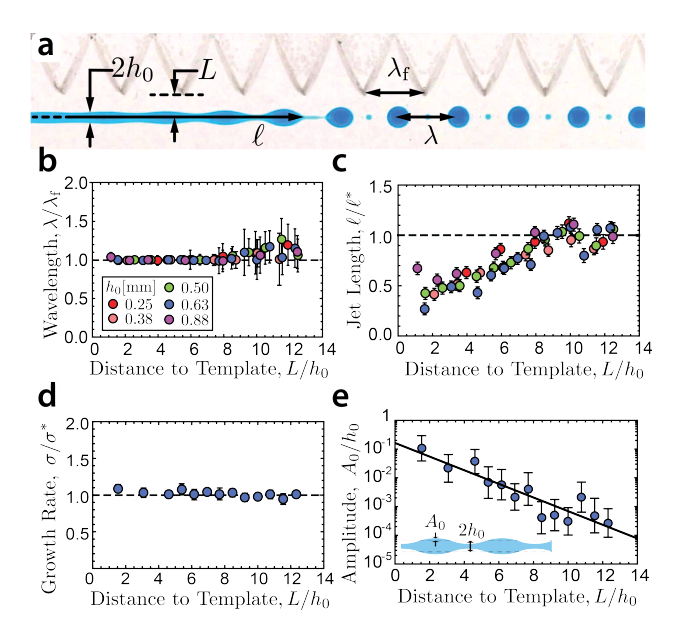


FIG. 2. **Enforcing a wavelength.** (a) Photograph of an experiment of a jet with radius h_0 printed at a distance L of an acrylic template (top view). (b) Breakup wavelength λ and (c) Jet length ℓ as a function of normalized distance to template L for different radius of injected jet h_0 . (d) Growth rate σ as a function of normalized distance to template L. Dashed line is the prediction from linear stability analysis. (e) Initial perturbation A_0/h_0 as a function of normalized distance to template L. Solid line is the best fit to the experimental data.

consistently low. These results suggest that the jet radius h_0 is the relevant lengthscale in this problem. This point is further confirmed by examining the length of the jet, ℓ , defined as the distance from the nozzle to the point where droplets are shedding. As evident from Fig. 2c, ℓ increases with L/h_0 until it reaches the limiting value ℓ^* of the unbounded case for $L/h_0 \sim 8$ [10]. To further quantify the role of the template and elucidate the mechanism at play, we measure the growth of the periodic perturbations leading to the jet breakup and compare the results to that of linear stability analysis where the jet radius is assumed to be $h(x,t) = h_0 + A_0 e^{\sigma t} \cos kx$ [3, 4, 36]. In Fig. 2d, we show that the observed growth rate σ is constant and independent of L. Therefore, the template does not affect the instability intrinsically. Rather, the template alters the initial conditions of the problem in the form of A_0 . A_0 is indirectly measured using the jet length data (see Methods). In Fig. 2e, we show that A_0 decreases exponentially as L increases. Close enough from the template, the jet is thus seeded with deformations significantly larger than the ambient noise and whose wavelength follows that of the template. As such, the breakup pattern locks with the template, thereby improving the droplet monodispersity.

With our solid templates we also demonstrate the possibility of enforcing wavelengths that deviate from the natural breakup wavelength λ^* . In Fig. 3a, typical breakup patterns with different template wavelengths $\lambda_{\rm f}$ are shown. As evident from the figure, the distance between drops is a complex function of that of the template. In particular, we observe locking in the range $0.7\lambda^* < \lambda_{\rm f} < 1.4\lambda^*$ as detailed next. When $\lambda_{\rm f} < 0.7\lambda^*$, the resulting breakup pattern is highly irregular with negligible locking effect, and the observed mean breakup wavelength remains close to λ^* (shown in Fig. 3b). In the range $0.7\lambda^* < \lambda_{\rm f} < 1.4\lambda^*$, the breakup wavelength λ follows $\lambda_{\rm f}$ closely. A much lower degree of polydispersity than that

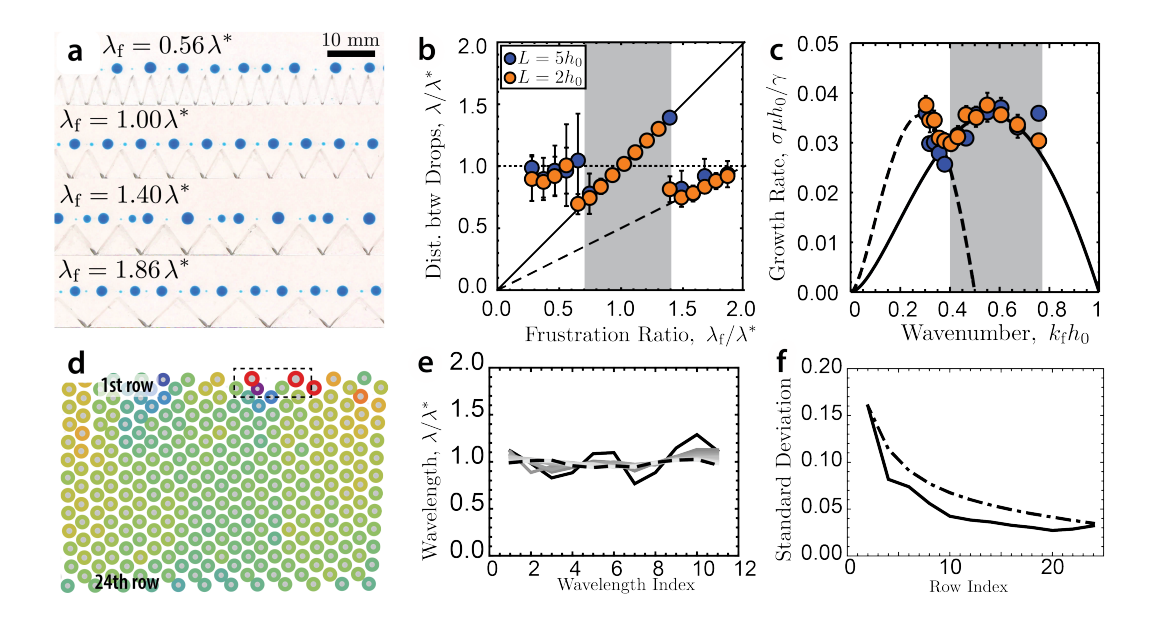


FIG. 3. Tuning the wavelength. (a) Photographs of jet breakup with initial radius $h_0 = 0.63$ mm and templates with different forcing wavelength λ_f ($L = 2h_0$). (b) Distance between the biggest drops λ/λ^* versus the frustration ratio λ_f/λ^* with $L = 5h_0$ and $2h_0$. The error bars correspond to the standard deviation of measurements. The grey band indicates the range of enforced wavelengths as determined experimentally. This range is reported in (c) where the corresponding growth rates are shown. The solid and dashed curves are the linear dispersion relations for the fundamental harmonic and superharmonic, respectively. (d) Self-correcting of wavelengths starting from a polydispersed row. The lattice pattern becomes more regular as rows are printed (e) The observed evolution of the wavelengths across the rows in (d). The 2nd and the 24th rows are shown by the solid and dotted lines, respectively. (f) Comparison of standard deviation in wavelength between the observed evolution (solid line) and the model prediction (dash-dotted line)

observed in unbounded breakups is observed, consistent with the aforementioned case $\lambda_f = \lambda^*$. The corresponding growth rate follows the prediction from linear stability analysis [35], which is plotted as the black curve in Fig. 3c. We also note that the satellite drops, i.e., the small drops in-between, become larger as λ_f increases. When close to the transitional value $\lambda_f \sim 1.4\lambda^*$, we observed unstable breakups yielding drops of varying sizes between the main drops (see Supplementary Figure 1). As λ_f is further increased, $\lambda_f > 1.4\lambda^*$, the breakup pattern becomes stable again, producing two large drops per forcing wavelength. In this superharmonic regime, the observed wavelength is half that of the forcing [37]. The dispersion relation for this superharmonic regime is plotted as the dashed curve in Fig. 3c and intersects the fundamental harmonic dispersion at $k_f h_0 = 0.37$, which gives a transition threshold ratio at $\lambda_f/\lambda^* = 1.51$. This value is close to the transition observed experimentally as shown in Fig. 3b and 3c. These results further confirm that the mechanism behind the wavelength locking effect is primarily underpinned by a modification of the initial conditions of the problem by the template. Remarkably, the remainder of the dynamics, e.g., the dispersion relation of the instability, appears to be unaffected by the template.

After describing the effects of a solid template, we now demonstrate that droplets them-

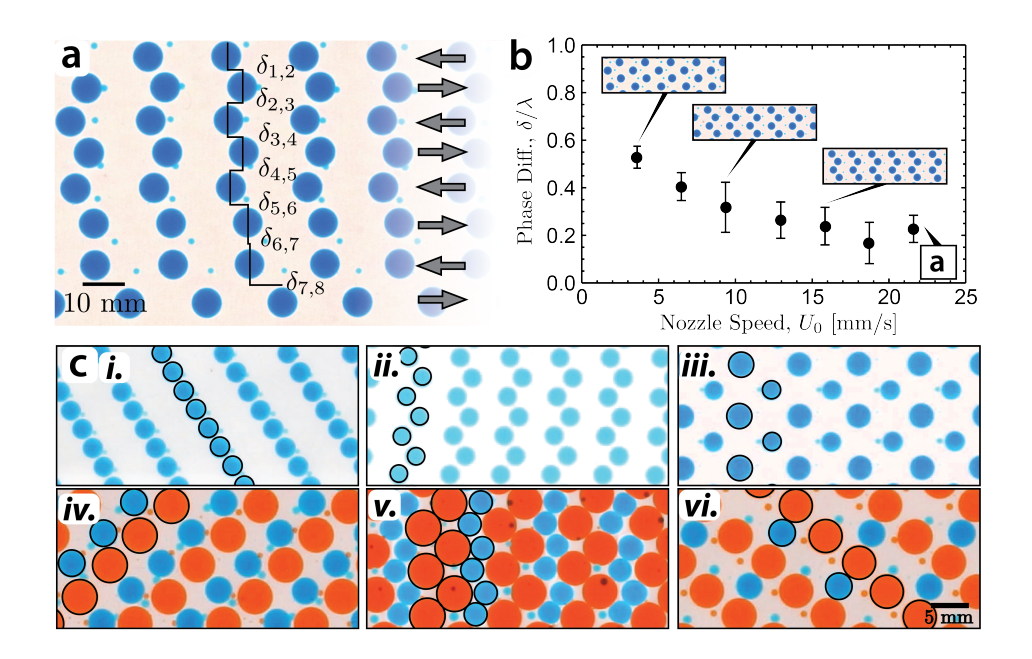


FIG. 4. **Designing complex patterns.** (a) Photograph of a crystal highlighting the phase difference between the drops in adjacent rows. Arrows indicate nozzle printing direction. (b) Final phase difference δ plotted as a function of nozzle speed U_0 . The drop radius and the separation between the rows are kept constant, R=3.5 mm and L=6.7 mm. The printing direction is reversed across the neighboring rows as shown in panel (a). (c) Drop patterns printed (i) $U_0=7.2$ mm/s, Q=0.25 mL/min, L=1.7 mm; (ii) $U_0=56.9$ mm/s, Q=1.98 mL/min, L=1.7 mm; (iii) $U_0=3.9$ and $V_0=0.25$ mL/min, $V_0=0.25$ mm/s, $V_0=0.25$ mL/min, $V_0=0.25$ mm/s, $V_0=0.25$ mL/min, $V_0=0.25$ mm/s, $V_0=0.25$ mm/s, $V_0=0.25$ mL/min, $V_0=0.25$ mm/s, $V_0=0.25$ mm/s, $V_0=0.25$ mL/min, $V_0=$

selves can serve as templates. When printing a thread next to a row of droplets with a well defined wavelength, we find that the breakup pattern follows the same wavelength (see Supplementary Video 2). As such, printing multiple lines parallel to a template leads to the emergence of a regular lattice of drops (see Supplementary Figure 2). Additionally, we have discovered that similar types of ordered droplet arrays also emerge when starting from a row whose breakup pattern is irregular, i.e., a self templating effect. In Fig. 3d, we show a typical droplet pattern observed when sequentially printing parallel threads without a solid template. The first row is unbounded and presents some polydispersity [10, 38]. As more rows are printed, the breakup progressively corrects itself such that a regular crystal-like pattern eventually emerges. In Fig. 3d, we circle the drops with color coding for their size. In particular, the distance between the two large drops in the first row (highlighted in the dotted box) is $\lambda \simeq 1.70\lambda^*$. In the next row, one wavelength is inserted such that the distance between drops is $\lambda = 0.95\lambda^*$. This observation is consistent with our previous discussion on the competition between harmonic modes. In this case, the smaller wavelengths are closer to the optimal value and thus grow faster than the large wavelength. From the second row onwards, there is no drastic change in the number of drops, and thus wavelength, but a subtle converging process continues. The rescaled wavelengths in every other row are shown in Fig. 3e. As evident from the figure, the initial non-uniformity in the pattern is progressively smoothed. We find that the convergence towards a lattice structure is iterative in nature and can be captured by a moving average model (see Methods and Fig. 3f). Any randomly distributed noise oscillating around a constant, here λ^* , therefore eventually vanish as evident from Fig. 3d-f. Likewise, the system also corrects localized defects, e.g., the intentionally seeded defects discussed in SI. In any case, a regular drop lattice is obtained regardless of the type of initial defect present.

We now turn to study the phase relationship between rows. An out-of-phase relation is typically observed in the simultaneous breakup of multiple liquid threads [11, 13, 39–41]. In contrast, our technique generates different phase relations as the lattice is the result of a dynamic process. The drops are indeed dragged long after they are formed when printing subsequent rows (see Supplementary Video 3). In Fig. 4a, we show the phase difference $\delta_{i,i+1}$, between consecutive lines i and i+1. These quantities evolve each time a line is added, e.g., $\delta_{7.8}(t+\Delta t)=\delta_{6.7}(t)$ owing to the periodic nature of the problem. Eventually, these values converge to the final phase difference δ , thus depending on the initial phase difference and successive shifts (see Supplementary Note and Supplementary Figures 5 - 7). As such, we are able to tune this quantity $0.2 < \delta/\lambda < 0.5$ by merely modifying the nozzle speed U_0 (see Fig. 4b for zig-zag printing patterns). Likewise, the relative printing direction between rows affects the overall pattern. In Fig. 4c, we show that a variety of drop crystals can be produced by adjusting injection flow rate, nozzle translation speed or changing the printing direction in different rows (Fig. 4c (i) - (ii)). Additionally, we leverage our understanding of the problem to produce complex patterns, e.g., with two populations of monodisperse drops (Fig. 4c (iv)-(vi)). To obtain such structures we print jets with different thread radii, h_1 and $h_2 \simeq 0.5 h_1$ (shown orange and blue, respectively). Stability analysis predicts that the natural breakup of such individual threads would yield wavelengths differing by a factor $2, \lambda_2 \simeq 0.5\lambda_1$. In stark contrast, we manage to force these wavelengths to be equal by templating (see Supplementary Video 4). First, the threads with radius h_1 are printed next to a solid template with wavelength $\lambda_{\rm f} \simeq 0.7 \lambda_1$ and yield a first set of drops (orange in the figure). This forcing matches the left boundary of the templating regin shown in Fig. 3b. Second, the threads with radius h_2 are printed just atop the already formed droplets. These droplets with wavelength $\lambda_{\rm f}$ now serve as templates for the breakup of the newly printed threads $\lambda_f \simeq 1.4\lambda_2$ (the right boundary of the templating domain in Fig. 3b). Since glycerol is denser than the surrounding oil, the blue droplets sink in between the orange ones. Using the same protocol, but changing the relative printing directions and inter-thread gap offers ways to tune the geometry of the final pattern as shown in Fig. 4c (iv)-(vi).

Discussion

In closing we note that our methodology can be applied to a broad range of fluids so long as jetting is possible [10]. As such, our approach is particularly suited to viscous liquids and polymer melts that cannot be handled by microfluidic devices and inkjet printers [42] but are necessary to materials science and many industrial applications [43]. Therefore, our methodology offers a new route for the fabrication of architected materials in a controllable and scalable manner. We envision the freedom in designing the pattern and its flexibility to be adapted to the existing droplet-based technologies will open up new opportunities as a tool of additive manufacturing.

Materials and Methods

Printing setup. Glycerol (99%, Avatar Corporation) is injected through a nozzle with inner radius r=0.85 mm into a reservoir fluid of silicone oil (DMS-T31, Gelest). The fluids have the same viscosity $\mu=1.1$ Pa.s and the interfacial tension between the fluids is $\gamma=0.028$ N/m. The flow rate, Q, is imposed using a syringe pump (Chemyx OEM) and we operate in the range 0.25 < Q[mL/min] < 4.41, such that the average injection speed at the nozzle is $1.8 < U_i = Q/\pi r^2[\text{mm/s}] < 32.4$. The nozzle is translated in the x, y-plane using a two-axis translational stage (AxiDraw V3.0) at speed $7.2 < U_0[\text{mm/s}] < 50.4$. The trajectory of the injector is controlled via a software (Inkscape).

Growth of perturbations on liquid threads. The initial stages of breakup are governed by linear theory [2, 4], such that the amplitude of perturbations on the thread grows exponentially. The growth rate σ can thus be estimated from an exponential fit to the temporal evolution of thread radius [38, 44].

We record the breakup of liquid threads at different distance L away from the solid template. The snapshots of the breakup evolution are binarized. The changes in greyscale at the thread center are measured over time to infer the change in light intensity and hence the growth of amplitude of the perturbations on the thread, according to the Beer-Lambert law. The growth rate σ can then be extracted from the evolution of the growing amplitude.

The initial amplitude of perturbations, A_0 is usually small (below 1 - 2% of the initial radius h_0) and cannot be measured accurately [44]. We estimate the ratio A_0/h_0 using the experimental measurements of jet length ℓ and growth rate σ :

$$\frac{A_0}{h_0} = e^{-\sigma t_b} = e^{-\sigma \ell/U_0} \tag{1}$$

Here t_b is the time needed to break the jet, which is given by the intact jet length divided by the nozzle speed U_0 [4, 10].

Moving average model. The converging process is akin to the dilution of variation or frustration in the system by a moving average kernel. In particular, with the kernel $(\frac{1}{2}, \frac{1}{2})$ the wavelengths in the later row are given by the average of the two closest neighboring wavelengths in the prior row. The process will repeat for the subsequent rows, resulting in increasingly more uniform breakup patterns (see Supplementary Note and Supplementary Figure 3). This model can be generalized to other kernels of the form $(\frac{1}{a}, \frac{a-1}{a})$ with similar results.

Acknowledgments

Funding: This work was supported by NSF via the grants NSF CAREER (CBET 2042930) and NSF FMRG (CMMI 2037097).

Competing of interest: The authors declare that they have no competing interests.

Authors contributions: PTB and JM designed the research. LC performed the experiments. All the authors analyzed the data and wrote the manuscript

Data availability: All data needed to evaluate the conclusions in the paper are present in the paper and/or the Supplementary Materials.

List of supplementary materials

Supplementary Information This file contains Supplementary Note and Supplementary Figure 1 - 7. Supplementary Video 1 This file contains Supplementary Video 1 (see legend Video 1). Supplementary Video 2 This file contains Supplementary Video 2 (see legend Video 2). Supplementary Video 3 This file contains Supplementary Video 3 (see legend Video 3). Supplementary Video 4 This file contains Supplementary Video 4 (see legend Video 4).

- [1] J. Plateau, Statique expérimentale et théorique des liquides soumis aux seules forces moléculaires, Vol. 2 (Gauthier-Villars, 1873).
- [2] L. Rayleigh, On the instability of jets, Proceedings of the London mathematical society 1, 4 (1878).
- [3] S. Tomotika, On the instability of a cylindrical thread of a viscous liquid surrounded by another viscous fluid, Proceedings of the Royal Society of London. Series A-Mathematical and Physical Sciences **150**, 322 (1935).
- [4] J. Eggers and E. Villermaux, Physics of liquid jets, Rep. Prog. Phys. 71, 036601 (2008).
- [5] R. Seemann, M. Brinkmann, T. Pfohl, and S. Herminghaus, Droplet based microfluidics, Reports on progress in physics **75**, 016601 (2011).
- [6] J. J. Kaufman, G. Tao, S. Shabahang, E.-H. Banaei, D. S. Deng, X. Liang, S. G. Johnson, Y. Fink, and A. F. Abouraddy, Structured spheres generated by an in-fibre fluid instability, Nature 487, 463 (2012).
- [7] J. Zhang, R. J. Coulston, S. T. Jones, J. Geng, O. A. Scherman, and C. Abell, One-step fabrication of supramolecular microcapsules from microfluidic droplets, Science **335**, 690 (2012).
- [8] B. G. Chung, K.-H. Lee, A. Khademhosseini, and S.-H. Lee, Microfluidic fabrication of microengineered hydrogels and their application in tissue engineering, Lab on a Chip 12, 45 (2012).
- [9] A. Fernandez-Nieves and A. M. Puertas, Fluids, colloids and soft materials: an introduction to soft matter physics (John Wiley & Sons, 2016).
- [10] L. Cai, J. Marthelot, and P.-T. Brun, An unbounded approach to microfluidics using the rayleigh-plateau instability of viscous threads directly drawn in a bath, Proceedings of the National Academy of Sciences 116, 22966 (2019).
- [11] P. Elemans, J. Van Wunnik, and R. Van Dam, Development of morphology in blends of immiscible polymers, American Institute of Chemical Engineers. AIChE Journal 43, 1649 (1997).
- [12] Y. M. Knops, J. J. Slot, P. H. Elemans, and M. J. Bulters, Simultaneous breakup of multiple viscous threads surrounded by viscous liquid, AIChE journal 47, 1740 (2001).
- [13] P. J. Janssen, H. Meijer, and P. Anderson, Stability and breakup of confined threads, Physics of Fluids 24, 012102 (2012).
- [14] M. Fermigier, L. Limat, J. Wesfreid, P. Boudinet, and C. Quilliet, Two-dimensional patterns in rayleigh-taylor instability of a thin layer, Journal of Fluid Mechanics **236**, 349 (1992).
- [15] J. Marthelot, E. Strong, P. M. Reis, and P.-T. Brun, Designing soft materials with interfacial instabilities in liquid films, Nature communications 9, 1 (2018).

- [16] Y. A. Vlasov, X.-Z. Bo, J. C. Sturm, and D. J. Norris, On-chip natural assembly of silicon photonic bandgap crystals, Nature **414**, 289 (2001).
- [17] B. A. Grzybowski, C. E. Wilmer, J. Kim, K. P. Browne, and K. J. Bishop, Self-assembly: from crystals to cells, Soft Matter 5, 1110 (2009).
- [18] A. G. Marin, H. Gelderblom, D. Lohse, and J. H. Snoeijer, Order-to-disorder transition in ring-shaped colloidal stains, Physical review letters **107**, 085502 (2011).
- [19] M. A. Boles, M. Engel, and D. V. Talapin, Self-assembly of colloidal nanocrystals: From intricate structures to functional materials, Chemical reviews 116, 11220 (2016).
- [20] G. Widawski, M. Rawiso, and B. François, Self-organized honeycomb morphology of star-polymer polystyrene films, Nature **369**, 387 (1994).
- [21] H. Yabu, M. Takebayashi, M. Tanaka, and M. Shimomura, Superhydrophobic and lipophobic properties of self-organized honeycomb and pincushion structures, Langmuir 21, 3235 (2005).
- [22] D. Shin, T. Huang, D. Neibloom, M. A. Bevan, and J. Frechette, Multifunctional liquid marble compound lenses, ACS applied materials & interfaces 11, 34478 (2019).
- [23] G. Villar, A. D. Graham, and H. Bayley, A tissue-like printed material, Science 340, 48 (2013).
- [24] H. J. Mea, L. Delgadillo, and J. Wan, On-demand modulation of 3d-printed elastomers using programmable droplet inclusions, Proceedings of the National Academy of Sciences 117, 14790 (2020).
- [25] P. R. Baraniak and T. C. McDevitt, Scaffold-free culture of mesenchymal stem cell spheroids in suspension preserves multilineage potential, Cell and tissue research **347**, 701 (2012).
- [26] S. Mashaghi, A. Abbaspourrad, D. A. Weitz, and A. M. van Oijen, Droplet microfluidics: A tool for biology, chemistry and nanotechnology, TrAC Trends in Analytical Chemistry 82, 118 (2016).
- [27] T. S. Kaminski, O. Scheler, and P. Garstecki, Droplet microfluidics for microbiology: techniques, applications and challenges, Lab on a Chip 16, 2168 (2016).
- [28] D. Beattie, K. H. Wong, C. Williams, L. A. Poole-Warren, T. P. Davis, C. Barner-Kowollik, and M. H. Stenzel, Honeycomb-structured porous films from polypyrrole-containing block copolymers prepared via raft polymerization as a scaffold for cell growth, Biomacromolecules 7, 1072 (2006).
- [29] A. Khelif, A. Choujaa, S. Benchabane, B. Djafari-Rouhani, and V. Laude, Guiding and bending of acoustic waves in highly confined phononic crystal waveguides, Applied physics letters 84, 4400 (2004).
- [30] R. H. Olsson III and I. El-Kady, Microfabricated phononic crystal devices and applications, Measurement science and technology 20, 012002 (2008).
- [31] H. Yabu and M. Shimomura, Simple fabrication of micro lens arrays, Langmuir **21**, 1709 (2005).
- [32] H. Ma, J. Cui, J. Chen, and J. Hao, Self-organized polymer nanocomposite inverse opal films with combined optical properties, Chemistry–A European Journal 17, 655 (2011).
- [33] M. A. Holden, D. Needham, and H. Bayley, Functional bionetworks from nanoliter water droplets, Journal of the American Chemical Society 129, 8650 (2007).
- [34] G. Maglia, A. J. Heron, W. L. Hwang, M. A. Holden, E. Mikhailova, Q. Li, S. Cheley, and H. Bayley, Droplet networks with incorporated protein diodes show collective properties, Nature nanotechnology 4, 437 (2009).
- [35] H. Stone and M. Brenner, Note on the capillary thread instability for fluids of equal viscosities, Journal of Fluid Mechanics **318**, 373 (1996).

- [36] F. Gallaire and P.-T. Brun, Fluid dynamic instabilities: theory and application to pattern forming in complex media, Philosophical Transactions of the Royal Society A: Mathematical, Physical and Engineering Sciences 375, 20160155 (2017).
- [37] G. Lerisson, P. G. Ledda, G. Balestra, and F. Gallaire, Instability of a thin viscous film flowing under an inclined substrate: steady patterns, Journal of Fluid Mechanics 898 (2020).
- [38] R. J. Donnelly and W. Glaberson, Experiments on the capillary instability of a liquid jet, Proceedings of the Royal Society of London. Series A. Mathematical and Physical Sciences **290**, 547 (1966).
- [39] Z. Zhang, G. Hilton, R. Yang, and Y. Ding, Capillary rupture of suspended polymer concentric rings, Soft Matter 11, 7264 (2015).
- [40] V. Mansard, J. M. Mecca, D. L. Dermody, D. Malotky, C. J. Tucker, and T. M. Squires, Collective rayleigh-plateau instability: A mimic of droplet breakup in high internal phase emulsion, Langmuir 32, 2549 (2016).
- [41] Q. Brosseau and P. M. Vlahovska, Streaming from the equator of a drop in an external electric field, Physical Review Letters 119, 034501 (2017).
- [42] A. B. Thompson, C. R. Tipton, A. Juel, A. L. Hazel, and M. Dowling, Sequential deposition of overlapping droplets to form a liquid line, Journal of Fluid mechanics **761**, 261 (2014).
- [43] H. Du, A. Cont, M. Steinacher, and E. Amstad, Fabrication of hexagonal-prismatic granular hydrogel sheets, Langmuir **34**, 3459 (2018).
- [44] E. Goedde and M. Yuen, Experiments on liquid jet instability, Journal of Fluid Mechanics 40, 495 (1970).